Journal of Computational Physics 378 (2019) 1–17

Contents lists available at ScienceDirect

Journal of Computational Physics

www.elsevier.com/locate/jcp

A hybrid smoothed dissipative particle dynamics (SDPD) spatial stochastic simulation algorithm (sSSA) for advection–diffusion–reaction problems

Brian Drawert [a,*,1], Bruno Jacob [b,1], Zhen Li [c], Tau-Mu Yi [d], Linda Petzold [b,e]

[a] Department of Computer Science, University of North Carolina at Asheville, Asheville, NC, 28804, USA
[b] Department of Mechanical Engineering, University of California-Santa Barbara, Santa Barbara, CA, 93106, USA
[c] Division of Applied Mathematics, Brown University, Providence, RI 02912, USA
[d] Department of Molecular, Cellular, and Developmental Biology, University of California-Santa Barbara, Santa Barbara, CA 93106, USA
[e] Department of Computer Science, University of California-Santa Barbara, Santa Barbara, CA, 93106, USA

ARTICLE INFO

Article history:
Received 4 May 2018
Received in revised form 26 October 2018
Accepted 27 October 2018
Available online 5 November 2018

Keywords:
Particle based fluid dynamics
Reaction–diffusion master equation
Discrete stochastic simulation

ABSTRACT

We have developed a new algorithm which merges discrete stochastic simulation, using the spatial stochastic simulation algorithm (sSSA), with the particle based fluid dynamics simulation framework of smoothed dissipative particle dynamics (SDPD). This hybrid algorithm enables discrete stochastic simulation of spatially resolved chemically reacting systems on a mesh-free dynamic domain with a Lagrangian frame of reference. SDPD combines two popular mesoscopic techniques: smoothed particle hydrodynamics and dissipative particle dynamics (DPD), linking the macroscopic and mesoscopic hydrodynamics effects of these two methods. We have implemented discrete stochastic simulation using the reaction–diffusion master equations (RDME) formalism, and deterministic reaction–diffusion equations based on the SDPD method. We validate the new method by comparing our results to four canonical models, and demonstrate the versatility of our method by simulating a flow containing a chemical gradient past a yeast cell in a microfluidics chamber.

1. Introduction

In recent years, the complexity of the models used to simulate systems in science and engineering has dramatically increased. These models span microscopic to macroscopic scales and multiple types of physics simulations, including fluid dynamics, solid mechanics, chemical reactions and transport, and thermodynamics. For systems in which the scales of time and space are sufficiently small (microscale), simulations are performed using molecular dynamics (MD) [1] with potential energy functions derived from classical mechanics. For macroscale systems involving a well-mixed system, a continuum approach (i.e., Navier–Stokes equations) is typically employed. At the intermediate mesoscale, recent work by Li et al. [2] has integrated reaction–diffusion of chemical species within a particle-based fluid dynamic framework. In the field of cell biology, it has been found that models with discrete stochastic dynamics are often required to recapitulate biologically

* Corresponding author.
E-mail address: bdrawert@unca.edu (B. Drawert).
[1] BD and BJ contributed equally to this work.

https://doi.org/10.1016/j.jcp.2018.10.043

relevant phenotypes [3]. Recent work has shown the importance of cellular level models with dynamic domain shapes and external flows coupled to discrete stochastic biochemical simulations [4,5].

Typically in fluid dynamics simulations, macroscale approaches based on continuum methods rely on the continuum hypothesis and local equilibrium assumptions. By considering volumes of particles as local thermodynamic systems, one can reduce the number of degrees of freedom by several orders of magnitude, because not all the scales of the system are resolved. This truncation of scales allows the simulation of larger systems for longer physical times. In this sense, continuum theories can be seen as coarse-grained versions of the atomic system [1].

The Knudsen number (Kn), defined as the ratio of the mean free path of the molecules being transported over a characteristic length scale [6], helps to determine whether it is meaningful to use a macroscopic approach. According to Karniadakis et al. [7], molecular effects become the dominant transport mechanism in fluid motion when $Kn \geq 10$. However, at the so-called transitional regime, $10^{-1} \leq Kn \leq 10^{1}$, several important phenomena involving molecular effects take place in complex systems [1] such as biological flows, and the behavior of polymers and colloids. In this regime, scales are considered mesoscopic, with spatio-temporal ranges in the interval $\mathcal{O}(10^{-9})$ – $\mathcal{O}(10^{-5})$ meters and $\mathcal{O}(10^{-9})$ – $\mathcal{O}(10^{-3})$ seconds [1], making the number of degrees of freedom required in a MD simulation currently impractical [8–10,1]. The most recent MD simulations are constrained to $\mathcal{O}(10^{9})$ atoms and up to $\mathcal{O}(10^{-9})$ seconds [10].

To capture the effect of a wide range of scales, researchers have developed methods that solve on one scale while modeling the others. For example, dissipative particle dynamics (DPD), proposed by Hoogerbrugge and Koelman [11] and later modified by Español and Warren [12], models mesoscale systems as a collection of particles which interact via a soft potential (conservative forces), while dissipative and stochastic forces provide the missing degrees of freedom of the formulation. The method has been applied to a wide range of problems in physics and chemistry [13] including heat transfer [14–16], reactive flows [2], flow through porous media [17,18] and shock-capturing [19,20].

Despite the success of DPD as a simple, robust and intuitive method, a number of conceptual shortcomings have been reported [8,21,10]. The lack of a direct connection between the model parameters and the physical parameters of the system is still an open area of research. As a consequence, DPD parameters must be calibrated on a case-by-case basis using empirical equations, often in a non-unique way [22,23,21]. Other shortcomings of the DPD method include the impossibility of imposing an equation of state directly in the model [21] and the risk of particle overlap due to the use of soft potentials [8].

These shortcomings of the DPD formulation were addressed by Español and Revenga [24], who proposed a generalization of the Smoothed Particle Hydrodynamics (SPH) method to model the hydrodynamics, along with an additional stochastic term to model the thermal fluctuations in the mesoscale. The resulting method, named Smoothed Dissipative Particle Dynamics (SDPD), inherits the benefits of second-order discretization of the Navier–Stokes equations in the Lagrangian form from SPH [8,9], along with the thermodynamic consistency of DPD [24]. For this method, transport coefficients and equations of state can be imposed as inputs directly in the model. Moreover, physical scales are consistent with the Navier–Stokes equations, and therefore hydrodynamic behavior is obtained.

In this paper we introduce a novel formulation of advection–diffusion–reaction in SDPD. For systems where the molecular discreteness is relevant, we propose to simulate the reaction–diffusion of species by use of the spatial stochastic simulation algorithm (sSSA) to resolve the reaction–diffusion master equation (RDME) [25–27]. An immediate advantage of the spatial stochastic approach is that transport of species is computed exactly, instead of approximately by adding a fluctuation term to the deterministic reaction–diffusion equations. On the other hand, in regions where small scales are negligible, we solve a deterministic form of the SDPD reaction–diffusion equation, thereby avoiding over-resolving scales and increasing computational efficiency.

Compared to mesh-based standard approaches, such as finite elements (FEM), finite differences (FDM) and finite volume (FVM) methods, the new hybrid sSSA-SDPD method introduced by this work presents important advantages. First, as a consequence of its Lagrangian description, the method allows the simulation of advection–diffusion–reaction systems with complex geometries without the need of using adaptive meshes or interface tracking. Additionally, the method is capable of simulating a broader range of problems, when compared with standard approaches. In particular, the method is well-suited for fluid flow problems where stochastic reactive–diffusive mass transport is relevant.

One class of problems in which the hybrid method is expected to excel compared to alternative approaches is the simulation of biological systems where advection and reaction–diffusion occur at different scales, ranging from the microscopic (e.g. stochastic molecular binding interactions) to the macroscopic (e.g. fluid flow). For example, a neutrophil in the blood can track down a single bacterium by sensing individual bacterial peptides that diffuse to and bind neutrophil receptors, triggering a biochemical response while experiencing the hydrodynamic forces from blood flow (Fig. 1). Physical forces, chemical reactions, diffusion, active transport, stochastic dynamics, and advection must all be modeled, which presents a formidable challenging for any computational framework. Commercial software solutions such as Comsol Multiphysics can capture the deterministic spatial dynamics but not the stochastic dynamics. The spatial stochastic simulation algorithm (sSSA) [28] simulates stochastic reaction–diffusion dynamics, but is ill-suited for representing fluid flow.

This paper is organized as follows: Section 2 briefly describes the SDPD and sSSA formulations. Section 3 focuses on the algorithmic description of the method proposed, with a discussion about its appropriate use in multiscale systems. Section 4 presents validations, applications and discussion of relevant results. Finally, conclusions and future perspectives are described in Section 5.

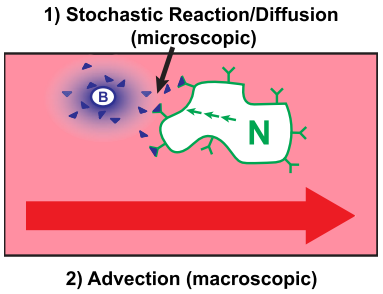

Fig. 1. Example of biological system possessing reaction, diffusion, advection, and stochastic dynamics. In an artery, a neutrophil (N) chemotaxes against the blood flow toward a bacterium (B) by sensing the gradient of individual bacterial peptides (blue triangles) that bind receptors (green Y-shapes) on the neutrophil cell surface. (For interpretation of the colors in the figure(s), the reader is referred to the web version of this article.)

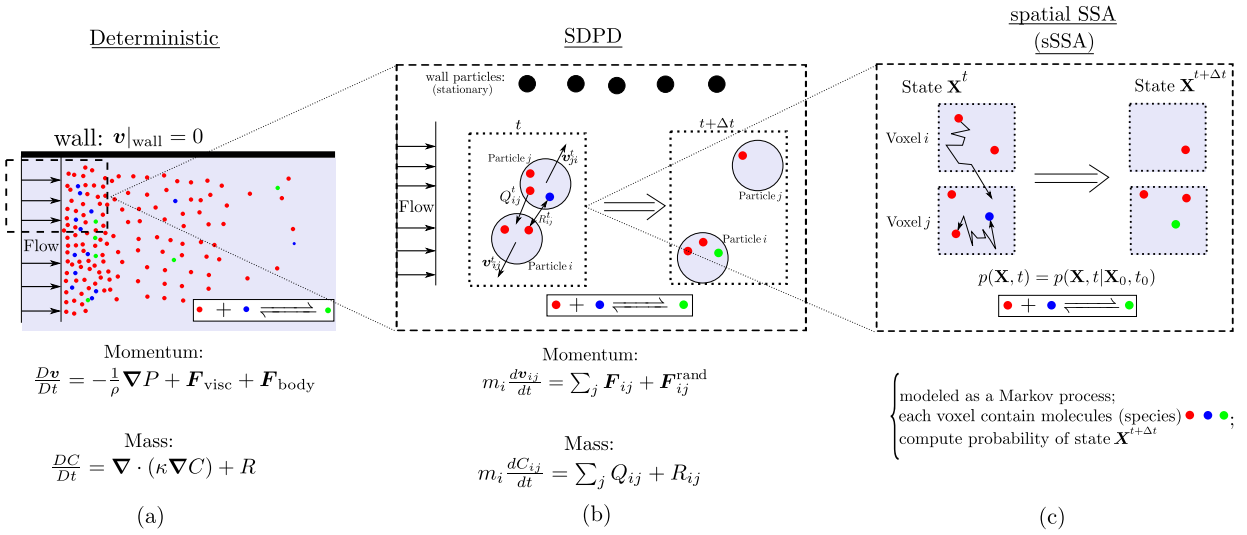

Fig. 2. Comparison between mathematical and physical models of (a) a typical deterministic approach, (b) SDPD, (c) sSSA, for the idealized case of a channel flow with diluted species. In the hybrid method, advection is solved using SDPD, while the mass transport can be solved using either a spatial stochastic algorithm or SDPD, depending if stochastic effects are relevant or not. In Figs. (a) and (b), the dotted parts denote magnified regions, illustrating the differences between the methods. In Fig. (b), v_{ij}, Q_{ij} and R_{ij} denote the pairwise velocity, flux of mass and reaction term, respectively. In Fig. (c), p in the Kolmogorov equation denotes the probability that the system can be found in state $\mathbf{X}$ at time t.

2. Background

The hybrid method addressed in this paper is based on the combination of two formulations: SDPD and SSA. In this section, we provide a brief theoretical overview of these two key elements in the proposed hybrid method. In SDPD [24], the domain is discretized as a finite number of particles, each representing a small volume of material that carries properties such as momentum, mass and energy. The position of the particles evolves in time according to some mechanistic model, such as the fluctuating Navier–Stokes equations for fluid flow [29]. In contrast, the sSSA algorithm [28] consists of a stochastic model for mesoscopic-scale stochastic reaction–diffusion kinetics, where the domain is discretized in voxels and the system is modeled as a Markov process. For each voxel, the number of molecules of diluted species characterize the state of the system that evolves in time according to the Kolmogorov equation.

The hybrid method proposed uses either the sSSA algorithm or the SDPD formulation to compute mass reaction–diffusion processes, and SDPD to compute advection and other body force dynamics. This is achieved by treating each particle in the system as a voxel for the sSSA. The immediate consequence of using the hybrid sSSA-SDPD method is the ability to correctly predict the dynamics of multiscale systems in an unified framework, resolving hydrodynamics and low-concentration reaction–diffusion systems at the same time.

An overview of the mathematical models of an arbitrary system from a deterministic, SDPD and hybrid method perspective is depicted in Fig. 2. For detailed formulations of SSA and SDPD, we refer the reader to the work of Gardiner et al. [28] and Español and Revenga [24], respectively.

2.1. SDPD

2.1.1. Theoretical aspects

Consider a domain $\Omega \subset \Re^3$, composed of a collection of particles representing fluid volumes, that evolve in time according to the isothermal Navier–Stokes equations and the reaction–diffusion equation:

$$\frac{D\rho}{Dt} = -\rho \nabla \cdot \boldsymbol{v}, \tag{1}$$

$$\frac{D\boldsymbol{v}}{Dt} = -\frac{1}{\rho}\nabla P + \boldsymbol{F}_{\text{visc}} + \boldsymbol{F}_{\text{body}}, \tag{2}$$

$$\frac{DC}{Dt} = \nabla \cdot (\kappa \nabla C) + R, \tag{3}$$

where ρ, $\boldsymbol{v}$, P, $\boldsymbol{F}_{\text{visc}}$, $\boldsymbol{F}_{\text{body}}$, C, κ and R denote the fluid density, velocity, pressure, viscous force, body force, concentration, mass diffusivity and reaction term, respectively. The $D(\cdot)/Dt$ operator denotes the material derivative [30], defined as

$$\frac{D(\cdot)}{Dt} = \frac{\partial(\cdot)}{\partial t} + \boldsymbol{v} \cdot \nabla(\cdot), \tag{4}$$

thus the characteristic curves of this operator are the particle trajectories [31]. Adopting a Lagrangian description, we consider each particle as a non-inertial frame of reference. Therefore, the advective acceleration term in Eq. (4), $\boldsymbol{v} \cdot \nabla(\cdot)$, vanishes identically, by virtue of having a zero relative velocity. Consequently, Eqs. (1)–(3) can be rewritten as:

$$\frac{\partial\rho}{\partial t} = -\rho \nabla \cdot \boldsymbol{v}, \tag{5}$$

$$\frac{\partial\boldsymbol{v}}{\partial t} = -\frac{1}{\rho}\nabla P + \boldsymbol{F}_{\text{visc}} + \boldsymbol{F}_{\text{body}}, \tag{6}$$

$$\frac{\partial C}{\partial t} = \nabla \cdot (\kappa \nabla C) + R. \tag{7}$$

Equations (5)–(7) show that the temporal variation of the variables of interest depends on the evaluation of spatial derivatives of these physical quantities. The solution of these equations numerically, therefore, raises the question of how to approximate the derivatives and transform these expressions into a set of algebraic equations involving the unknowns of the problem [31,32].

In Eulerian-based methods, at each time step, points of space are arbitrarily selected as inertial frames of reference and therefore the spatial grid spacing is, in general, fixed; thus, derivatives are typically piecewise-approximated using linear functions, polynomials, etc. In contrast, in a Lagrangian-based method, since particles are moving along with the flow, the evaluation of derivatives involves interpolation processes, usually based on radial smoothing kernel functions [31].

In order to find a good candidate for the interpolation process, consider a continuous function $f(\boldsymbol{x})$, defined at coordinates $\boldsymbol{x}$. Consider the following identity [32]

$$f(\boldsymbol{x}) = \int_{\Omega} f(\boldsymbol{x}')\delta(\boldsymbol{x} - \boldsymbol{x}')dx', \tag{8}$$

where $\delta(\boldsymbol{x} - \boldsymbol{x}')$ is the Dirac delta function. Due to the infinitesimal support of the Dirac function and the finite decimal precision of computers, it is not possible to write a discrete numerical method using this integral representation of a function. In order to overcome this limitation, SPH theory approximates Eq. (8) by replacing the Dirac function with a smoothing kernel function W with finite support h

$$f(\boldsymbol{x}) \approx \int_{\Omega} f(\boldsymbol{x}')W(\boldsymbol{x} - \boldsymbol{x}', h)dx'. \tag{9}$$

Note that Eq. (9) is an approximation. The accuracy of the approximation depends on the choice of W. In the SPH literature, the smoothing kernel function is often chosen based on three conditions [17,33]: a) the normalization of the smoothing function, that requires its integral to be identically one in the volume Ω; b) the Dirac delta condition, which requires that $W(\boldsymbol{x} - \boldsymbol{x}', h) \to \delta(\boldsymbol{x} - \boldsymbol{x}')$ as the support h approaches zero; c) kernel compactness, which guarantees that $W = 0$ outside of its support.

After judiciously choosing a function W, the next step consists of rewriting the integral approximation given by Eq. (9) as a discrete sum. The domain Ω is then discretized using N particles, each located at coordinates $\boldsymbol{x}_i$

$$\langle f(x_i)\rangle = \sum_{j=1}^{N} m_j \frac{f_j}{\rho_j} W(\boldsymbol{x}_i - \boldsymbol{x}_j), \tag{10}$$

where m_j and $\langle f_j \rangle$ denote the mass of particle j and the kernel approximation of the field $f(\boldsymbol{x})$ at position $\boldsymbol{x}_j$, respectively. As a consequence of the SPH formulation, since m_j and f_j are defined locally (i.e., they are particle properties), linear operators (such as the gradient) will affect only the weight function. Therefore, the gradient of f is given by

$$\langle \nabla f(x_i) \rangle = \sum_{j=1}^{N} m_j \frac{f_j}{\rho_j} \nabla W(\boldsymbol{x}_i - \boldsymbol{x}_j), \tag{11}$$

where the resulting directional gradient operator is evaluated as

$$\nabla W(\boldsymbol{x}_i - \boldsymbol{x}_j) = \frac{\boldsymbol{x}_{ij}}{x_{ij}} \frac{dW(\xi)}{d\xi}, \tag{12}$$

with $\boldsymbol{x}_{ij} = \boldsymbol{x}_i - \boldsymbol{x}_j$, $x_{ij} = ||\boldsymbol{x}_{ij}||_2$ and ξ denoting a generalized coordinate. In this work, we have adopted the Lucy kernel, proposed by Lucy [34], with $\xi = x_{ij}/h$

$$W(\xi) = \begin{cases} \alpha_D (1+3\xi)(1-\xi)^3, & \text{if } 0 \le \xi \le 1, \\ 0, & \text{otherwise}, \end{cases} \tag{13}$$

where the normalization parameter α_D depends on the number of dimensions of the problem

$$\alpha_D = \begin{cases} 5/4h, & \text{if 1D}, \\ 5/\pi h^2, & \text{if 2D}, \\ 105/16\pi h^3, & \text{if 3D}. \end{cases} \tag{14}$$

We proceed now by applying this methodology to Eqs. (5)–(7). The derivation of the deterministic part of the mathematical model, i.e., the SPH formulation, can be found in Monaghan [31]. For a complete derivation of the SDPD method and stochastic hydrodynamic thermal equations, the reader may refer to Español and Revenga [24]. In addition, a detailed discussion of the stochastic generalization of advection–diffusion equations, along with the exact specification of random terms for the SDPD concentration fields, can be found in Ellero et al. [35].

The resulting equations, disregarding body forces, are given by

$$\frac{d\rho}{dt} = -\sum_{j=1}^{N} m_j \left(\boldsymbol{v}_{ij} \cdot \boldsymbol{x}_{ij}\right) \frac{1}{x_{ij}} \frac{dW}{d\xi}, + \xi h c_0 \sum_{j=1}^{N} \boldsymbol{\psi}_{ij} \cdot \boldsymbol{x}_{ij} \frac{1}{x_{ij}} \frac{dW}{d\xi} \tag{15}$$

$$\frac{d\boldsymbol{v}}{dt} = \left[-\sum_{j=1}^{N} m_j \left(\frac{P_i}{\rho_i^2} + \frac{P_j}{\rho_j^2} \right) \frac{1}{x_{ij}} \frac{dW}{d\xi} \right] + \left[\frac{5\eta}{3} \sum_{j=1}^{N} \frac{1}{x_{ij}^3} \frac{dW}{d\xi} \frac{\boldsymbol{v}_{ij} + \left(\boldsymbol{v}_{ij} \cdot \boldsymbol{x}_{ij}\right) \boldsymbol{x}_{ij}}{\rho_i \rho_j} \right] + \frac{d\tilde{\boldsymbol{v}}}{dt}, \tag{16}$$

$$\frac{dC}{dt} = \left[-\sum_{j=1}^{N} m_j \frac{(\kappa_i + \kappa_j)(C_i - C_j)}{\rho_i \rho_j x_{ij}} \frac{dW}{d\xi} \right] + \frac{d\tilde{C}}{dt}. \tag{17}$$

In Eq. (15), $\boldsymbol{\psi}_{ij}$ and ξ denote the artificial density diffusion and its amplitude, respectively. This correction was proposed by Molteni and Colagrossi [36], as a way to reduce the numerical noise in the pressure valuation for weakly-compressible SPH, and has the form

$$\boldsymbol{\psi}_{ij} = 2 \left(\frac{m_i \rho_j}{m_j \rho_i} - 1 \right) \frac{\boldsymbol{x}_{ij}}{x_{ij}^2 + \varepsilon_h h^2}, \tag{18}$$

where $\varepsilon_h \sim 0.01$ is a small scalar set to prevent numerical singularities [31,37]. Considering the significant improvements presented by Molteni and Colagrossi [36] in terms of stability, we have taken the amplitude of the artificial density diffusion to be $\xi = 0.1$. Alternatively to the continuity equation, Eq. (15), it is possible to compute the density via interpolation, as

$$\rho_i = \sum_{j=1}^{N} m_j W_{ij}. \tag{19}$$

Although tests show that Eqs. (15) and (19) are equivalent [38], it is worth mentioning that the continuity equation, Eq. (15), provides the computational advantage of allowing the rates of change of all physical variables to be computed in one single loop. In the other hand, Eq. (15) carries the disadvantage that mass conservation is not preserved [38]. Another important aspect of Eq. (15) is that this equation is deterministic, whereas Eqs. (16)–(17) are strictly compliant with the GENERIC [39,40] framework. For a fully GENERIC-compliant system of equations, the reader might consider using Eq. (19)

[24]. Based on its computational advantages and the increased numerical stability achieved by the artificial density diffusion of Molteni and Colagrossi [36], we have adopted Eq. (15).

The random terms $d\tilde{\boldsymbol{v}}/dt$ are introduced in the equations as a tensorial generalization of a stochastic Wiener process [21],

$$\frac{d\tilde{\boldsymbol{v}}}{dt} = \sum_{j=1}^{N} \left[\left(\frac{40}{3} \frac{\eta \kappa_B T_0}{\rho_i \rho_j} \frac{dW}{d\xi} \right)^{1/2} \frac{d\widehat{\mathbf{W}}_{ij}}{dt} \cdot \frac{\boldsymbol{x}_{ij}}{x_{ij}} \right], \tag{20}$$

where

$$d\tilde{\mathbf{W}}_{ij} = \frac{\tilde{\mathbf{W}}_{ij} + \tilde{\mathbf{W}}_{ij}^T}{2}, \tag{21}$$

is the symmetric part of a matrix of independent increments in the Wiener process [21], κ_B is the Boltzmann constant and T_0 is a characteristic temperature of the system. For the random term in the reaction–diffusion equation, we follow the assumptions described by Li et al. [2], that disregard the influence of the random term in diffusive processes, based on the fact that the mass of a single solute molecule $m_{s,i}$ is small compared to the mass of the SDPD particle m_i. Therefore, we assume that $d\tilde{C} \ll dC$.

In order to close the model described by Eqs. (15)–(17), a relationship between density and pressure field must be established. In the Lagrangian fluid dynamics literature, two different approaches are widely used: 1) treat the flow as incompressible, either by solving a pressure-Poisson equation to obtain a divergence-free velocity field [37,41], or by requiring as a kinematic constraint that the volume of the fluid particles is constant [42]; or 2) treat it as weakly compressible, and impose an equation of state [34,38,21,43,33].

In the present work, we followed the classical weakly-compressible SPH approaches, where the pressure of a fluid particle is obtained from the density field using an equation of state [44]. A common choice is the so-called Tait's equation of state [45,43,33]:

$$p = p_0 \left[\left(\frac{\rho}{\rho_0} \right)^{\gamma} - 1 \right], \tag{22}$$

where p_0, ρ_0 denote reference pressure and density, respectively, and γ is the polytropic constant. It is a common practice [43,33] to select $p_0 = \rho_0 c_0^2/\gamma$, where c_0 is the artificial speed of sound. In order to limit density variations to 1%, we choose $\gamma = 7$. Here, c_0 is chosen such that it is at least two orders of magnitude higher than the characteristic velocity of the problem.

2.1.2. Numerical aspects

Following several authors [46,36,44], the integration of Eqs. (15)–(17) was performed using a two-step predictor–corrector scheme. Specifically, considering $\boldsymbol{Y} = [\boldsymbol{v}_i, \rho_i, C_i]$ the vector of unknowns of the system

$$\frac{\partial \boldsymbol{Y}}{\partial t} = f(\boldsymbol{Y}, t), \tag{23}$$

the explicit trapezoidal method is given by

$$\begin{aligned} \tilde{\boldsymbol{Y}} &= \boldsymbol{Y}^{n-1} + \Delta t f(t^{n-1}, \boldsymbol{Y}^{n-1}), \\ \boldsymbol{Y}^{n} &= \boldsymbol{Y}^{n-1} + \frac{\Delta t}{2} \left(f(t^{n-1}, v^{n-1}) + f(t^{n}, \tilde{\boldsymbol{Y}}) \right), \end{aligned} \tag{24}$$

which requires the evaluation of f only once per time step. A necessary condition for stability, given by the Courant–Friedrichs–Lewy condition based on the artificial speed of sound c_0, was used to estimate a suitable time step Δt for each simulation [33].

2.2. SSA and RDME

It has been observed that mean-field or deterministic models are often insufficient to capture the relevant dynamics of many biological systems [47–49]. At this cellular level, biochemical systems in which the copy number of any relevant chemical species is sufficiently small can be more accurately modeled with discrete stochastic simulation, of which the most popular method is the Stochastic Simulation Algorithm (SSA) or Gillespie algorithm [50]. The SSA assumes that the system is spatially homogeneous, or well-mixed. To model spatially inhomogeneous stochastic biochemical systems at the mesoscopic scale, reaction–diffusion master equation (RDME) [28]-based methods discretize space into spatially homogeneous voxels [25–27] are often used. In our spatial SSA (sSSA), we integrate the RDME-based methods with a particle-based fluid dynamics simulation framework by using each SDPD particle as a RDME voxel. Thus, the stochastic chemical reactions are solved within each of the SDPD particles, and the stochastic diffusion are solved between each of the SDPD particles.

Algorithm 1 SSA Reactions.

Input: Current population of species in each particle: $\mathbf{X}_{is}$, Set of SSA reactions $r \in R$ and propensity functions $a_r(\mathbf{X}_{i*})$, Integration timestep τ_{step}
Output: Population of each SSA species in each particle at time $t + \tau_{step}$.
1: Calculate $a_{ir} = a_r(\mathbf{X}_{i*})$; $a_0 = \sum_i \sum_r a_{ir}$
2: $t' = 0$; $r_1, r_2 \in URN(0,1)$; $t' += -\log(r1)/d_0$
3: **while** $t' < t_{split}$ **do**
4: Find: $\max_{\mu_i \mu_r} \left[a_0 r_1 > \sum_i^{\mu_i} \sum_r^{\mu_r} a_{ir}\right]$
5: $\mathbf{X}_{\mu_i \mu_s} += \nu_{\mu_i \mu_r}$
6: Update: a_{ir}, a_0
7: $r_1, r_2 \in URN(0,1)$
8: $t' += -\log(r1)/a_0$
9: **end while**

The spatial SSA algorithm is based in the Reaction–Diffusion Master Equation (RDME) formalism [28]. The RDME is a mathematical model for spatially-resolved mesoscopic-scale stochastic chemical reaction–diffusion kinetics. It gives the time evolution of the probability distribution for the state of the system. First, the physical domain is partitioned into K non-overlapping subvolumes or voxels, similar to numerical methods for PDEs. Molecules are taken to be point particles and the state of the system is the discrete number of molecules of each species for each of the voxels in the domain. Modeling the reaction–diffusion dynamics as a Markov process gives the following forward Kolmogorov equation for the time evolution of $p(\mathbf{X}, t) = p(\mathbf{X}, t|\mathbf{X}_0, t_0)$ (the probability that the system can be found in state $\mathbf{X}$ at time t, conditioned on the initial condition $\mathbf{X}_0$ at time t_0)

$$\frac{\partial p(\mathbf{X}, t)}{\partial t} = \mathcal{R}p(\mathbf{X}, t) + \mathcal{D}p(\mathbf{X}, t), \tag{25}$$

$$\mathcal{R}p(\mathbf{X}, t) = \sum_{i=1}^{K} \sum_{r=1}^{M} a_{ir}(\mathbf{X} - \nu_{ir}) p(\mathbf{X} - \nu_{ir}, t) - a_{ir}(\mathbf{X}) p(\mathbf{X}, t), \tag{26}$$

$$\mathcal{D}p(\mathbf{X}, t) = \sum_{s=1}^{S} \sum_{i=1}^{K} \sum_{j=1}^{K} d_{sij}(\mathbf{X} - \mu_{sij}) p(\mathbf{X} - \mu_{sij}, t) - d_{sij}(\mathbf{X}) p(\mathbf{X}, t), \tag{27}$$

where $\mathbf{X}$ is a $K \times S$ state matrix, and S is the number of chemical species. The functions $a_{ir}(\mathbf{X}_i)$ define the propensity functions of the M chemical reactions, and ν_{ir} are stoichiometry vectors associated with the reactions. The propensity functions are defined such that $a_{ir}(\mathbf{X})\Delta t$ gives the probability that reaction r occurs in a small time interval of length Δt. The stoichiometry vector ν_{ir} defines the rules for how the state changes when reaction r is executed. $d_{ijs}(\mathbf{X}_i)$ are propensities for the diffusion jump events, and μ_{ijs} are stoichiometry vectors for diffusion events. μ_{ijs} has only two non-zero entries, corresponding to the removal of one molecule of species X_s in voxel i and the addition of a molecule in voxel j. The propensity functions for the diffusion jumps, d_{ijs}, are selected to provide a consistent and local discretization of the diffusion equation.

We do not solve the RDME directly. Instead, we generate sample paths of the underlying stochastic process. The SSA does this by generating two random numbers on each time step r_1 and r_2. These determine which reaction event r will fire next and at what time τ it will fire. These are based on the probabilistic reaction rates (called *propensities*). Then the system state is updated by applying the stoichiometry vector ν_{*r} for reaction r to the state vector $\mathbf{X}$. The propensity functions are updated, the time is incremented by τ, and the procedure continues until the final time. This procedure is shown in Algorithm 1.

For SSA diffusion, we use a $K \times K$ matrix, the diffusion matrix $\mathcal{D}$, where $\mathcal{D}_{ij}$ is the diffusion propensity for molecules to jump from particle i to particle j. Following the formulation of Tartakovsky et al. [51], it is defined as:

$$\mathcal{D}_{ij} = \begin{cases} -2\frac{m_i m_j}{m_i + m_j} \frac{\rho_i + \rho_j}{\rho_i \rho_j} \frac{x_{ij}^2}{x_{ij}^2 + \varepsilon_h h^2} \frac{dW}{d\xi}, & \text{if } i \neq j, \\ -\sum_{n, n \neq j} \mathcal{D}_{nj}. & \text{if } i = j. \end{cases} \tag{28}$$

This procedure to solve the SSA diffusion over a time interval $[t, t + \tau_{step}]$ is shown in Algorithm 2.

3. Proposed method

3.1. Overview

The goal of the proposed hybrid method is to provide an alternative framework, for the simulation of multiscale systems that potentially involve a broad spectrum of Knudsen numbers, involving micro-, meso- and macro-scopic scales. In this sense, advection–diffusion–reaction problems could be resolved by the same method and numerical solver, without the burden of over-resolving small scales when not needed, nor truncating fluctuations in meso/microscale regimes.

Algorithm 2 SSA diffusion.

Input: Current particle positions: $\boldsymbol{x}_i$, Current population of species in each particle: $\mathbf{X}_{is}$, Set of SSA species diffusion coefficients: κ_{ijs}, Integration timestep τ_{step}

Output: Population of each SSA species in each particle at time $t + \tau_{step}$.

Create flux $K \times S$ matrix $\mathcal{Q} = 0$
Calculate diffusion matrix $\mathcal{D}$ [Eq. (28)]
Calculate $d_{ijs} = \kappa_{ijs}\mathcal{D}_{ij}\mathbf{X}_{is}$; $d_0 = \sum_i \sum_j \sum_s d_{ijs}$
$t' = 0$; $r_1, r_2 \in URN(0, 1)$; $t' \mathrel{+}= -\log(r1)/d_0$
while $t' < t_{split}$ **do**
  Find: $\max_{\mu_i \mu_j \mu_s} \left[d_0 r_1 > \sum_i^{\mu_i} \sum_j^{\mu_j} \sum_s^{\mu_s} d_{ijs} \right]$
  $\mathbf{X}_{\mu_i \mu_s} --$; $\mathcal{Q}_{\mu_i \mu_s} --$; $\mathcal{Q}_{\mu_j \mu_s} ++$
  Update: d_{ijs}, d_0
  $r_1, r_2 \in URN(0, 1)$
  $t' \mathrel{+}= -\log(r1)/d_0$
end while
$\mathbf{X}_{is} \mathrel{+}= \mathcal{Q}_{is} \forall i, s$

Algorithm 3 Hybrid SDPD-SSA method.

Input:
Domain region and boundary conditions,
Initial Particle Positions/masses/velocities,
Particle pair interactions,
Set of SDPD species: diffusion coefficients & initial concentrations,
Set of SDPD reactions,
Set of SSA species: diffusion coefficients & initial populations,
Set of SSA reactions,
Integration timestep τ_{step}, h, ρ, e, t_{final}

Output: At each sample time, for each particle: position, velocity, concentration of each SDPD species, population of each SSA species.

$t = 0$
while $t < t_{final}$ **do**
  Solve for new position of SDPD particles [Eq. (15)]
  Solve for new velocity of SDPD particles [Eq. (16)]
  Solve deterministic reaction–diffusion [Eq. (17)]
  Solve SSA reactions [Algorithm 1]
  Solve SSA diffusion [Algorithm 2]
  $t = t + \tau_{step}$
end while

The algorithm treats advection via the Navier–Stokes equations using the SDPD formulation, and reaction–diffusion by either SSA, SDPD or both. Coupling between advection and diffusion with body forces, e.g., in natural convection phenomena, take place via SSA or SDPD diffusion, depending on the nature of the problem.

As described in Eq. (15), the SDPD formulation includes a random force term, and the momentum equation is then treated as a stochastic differential equation (SDE). Depending on the Knudsen number, random effects might be relevant or not. For instance, consider a flow of red blood cells: in a macroscale regime, the effects of the random force do not change significantly the bulk motion that is transporting the cells; therefore, the force term might be disregarded and the SDPD equations are reduced to the standard SPH formulation. For the transport inside one of the cells, however, diffusion occurs in a meso/microscale regime, and thus SSA could be used to resolve interactions.

3.2. Algorithm

Our algorithm utilizes a first order operator splitting method to decouple and simultaneously solve the SDPD fluid dynamics, the SDPD deterministic reaction–diffusion, and the SSA stochastic reaction–diffusion equations over the same time interval $[t, t + \tau_{step}]$. First, we time integrate equations (15), (16), and (17) over the interval using an explicit trapezoidal method. Then, we execute the SSA chemical reaction simulation [Algorithm 1] within each voxel/SDPD particle. Finally, we execute the SSA diffusion simulation [Algorithm 2] between all voxel/SDPD particles. The procedure to solve the full system is shown in Algorithm 3.

3.3. Implementation

The hybrid method summarized in Algorithm 3 was implemented in a stable version of the open-source Large-scale Atomic/Molecular Massively Parallel Simulator (LAMMPS) [52] (v. 11 Aug. 2017). LAMMPS was originally developed as a molecular dynamics code, but its portability allow the implementation of new methods and particle interactions without modifying the kernel of the code, responsible for the efficient link-cell and neighbor list of the particles.

Our source code is available at the Github page: https://github.com/briandrawert/hybrid_SSA_SDPD.

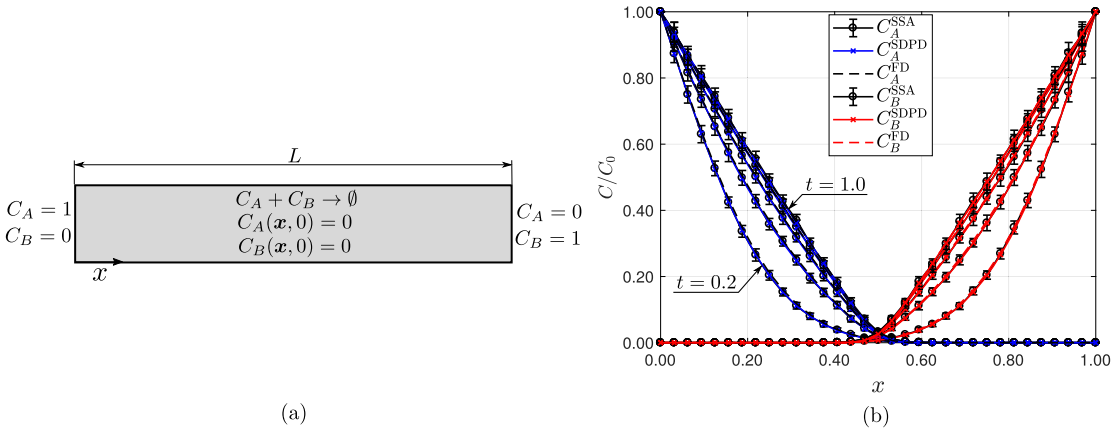

Fig. 3. (a) Schematic of degradation reaction of two arbitrary species, with initial and boundary conditions. (b) Plot of the concentration of the chemical species along the length of the cylindrical domain, at $t = 0.2, 0.4, 0.6, 0.8$ and 1.0 [s] for $N = 33$ particles.

4. Results

In this section we provide experimental validations of the proposed hybrid method. Section A discusses a one-dimensional, stationary reaction–diffusion problem, and Section B compares results of a classical advection–diffusion problem with the literature. Validations for 1D and 2D diffusion are provided in Drawert et al. [53].

4.1. Validation for one-dimensional reaction–diffusion

The diffusion cases presented so far validated the diffusion treatment with sSSA and SDPD for Dirichlet boundary conditions. We now proceed by allowing reactions of different species to take place. The following test case was also used in the validation of the software Stochastic Simulation Service (StochSS [54]), for the case of a three-dimensional cylinder. For this case, all the physical parameters are expressed in SI units.

Consider a domain $\Omega = [0, 1]$, with non-homogeneous Dirichlet boundary conditions imposed in the left and right walls. The walls are constrained with imposed concentrations arbitrary species C_A and C_B, as depicted in Fig. 3a. The initial conditions are homogeneous, $C_A(\boldsymbol{x}, t = 0) = C_B(\boldsymbol{x}, t = 0) = 0$, $\forall \boldsymbol{x} \in \Omega \mid \boldsymbol{x} \neq \partial\Omega$.

Species C_A and C_B interact with each other via mass action at a constant kinetic rate k_{AB}, leading to annihilation, i.e., $C_A + C_B \xrightarrow{k_{AB}} \emptyset$. The mathematical model that describes the system is given by

$$\frac{\partial}{\partial t}\begin{bmatrix} C_A \\ C_B \end{bmatrix} = \begin{bmatrix} \kappa_A & 0 \\ 0 & \kappa_B \end{bmatrix} \frac{\partial^2}{\partial x^2}\begin{bmatrix} C_A \\ C_B \end{bmatrix} + \begin{bmatrix} R_A \\ R_B \end{bmatrix}, \tag{29}$$

where κ_A, κ_B are the mass diffusivities, and R_A, R_B denote the reaction source terms. Based on the law of mass action, the reaction terms are given by

$$\begin{bmatrix} R_A \\ R_B \end{bmatrix} = \begin{bmatrix} -k_{AB} C_A C_B \\ -k_{AB} C_A C_B \end{bmatrix}, \tag{30}$$

The resulting system is a set of non-linear, coupled, second-order partial differential equations. Since there is no systematic way of obtaining the exact solution of this initial-boundary value problem, we propose its validation using high-fidelity numerical data as reference. Thus, we performed the validation using in-house code that solves the aforementioned problem using a 6th order tridiagonal compact finite-difference scheme [55], with grid spacing equivalent to the distance between particles used in the spatial SSA and SDPD simulations. The source code for our implementation of this solver is included as a file in the Supplementary Material.

Numerical simulations were performed using mass diffusivities $\kappa_A = \kappa_B = 0.1$ [m^2/s] and reaction kinetic rate $k_{AB} = 0.1$ [s^{-1} molecules^{-1}]. Three levels of spatial refinement were used: 17, 33 and 65 equally-spaced particles, spaced $\Delta x = 1/16, 1/32, 1/64$ [m] of each other, respectively. A comparison of the concentration profiles solved using SSA and SDPD and contrasted with the compact finite difference solution is shown in Fig. 3b. SSA solutions were obtained as an average of $N_r = 100$ realizations.

Results shown good agreement with the high-order reference solution. As expected, concentration curves monotonically decrease towards the half-length of the domain, due to the symmetric nature of the problem.

Table 1 summarizes the errors for each simulation. Errors with SSA and SDPD showed the same order of magnitude, which indicates that SSA-based reaction–diffusion is able to accurately predict the physics of the problem. This result, along with the diffusion validations, indicates that there is no penalty in using SSA except for the burden of over-resolving scales,

Table 1
Estimated errors of reaction–diffusion in a cylinder.

Δx	N	ϵ^{SDPD} [a]	ϵ^{SSA} [b]	C_0
1/16	17	1.856×10^{-4}	7.285×10^{-4}	1.6×10^5
1/32	33	1.698×10^{-4}	5.334×10^{-4}	3.2×10^5
1/64	65	2.325×10^{-4}	6.644×10^{-4}	6.4×10^5

[a] Error computed at steady-state, $t = 100$.
[b] Error computed based at the mean profile of $N_r = 100$ at steady-state.

which increases the computational effort. However, notice that the opposite is not true, i.e., the usage of a deterministic approach does not necessarily reproduce the physics of the problem, as stochastic effects are relevant for $Kn \geq 10^{-1}$. Thus, our method allows the simulation of cases even when it is not clear whether the stochastic effects are relevant or not, covering the whole spectrum of Knudsen numbers.

4.2. Validation for natural convection in a cylinder inside a square enclosure

The final validation case consists of comparing flow effects (advection), resolved via SDPD, and molecular transport (diffusion), resolved with both SSA and SDPD.

Instead of treating diffusion as a passive scalar, as in the validation of the tDPD model [2], the present work proposes the validation of advection–diffusion using a coupling force, based on the Oberbeck-Boussinesq approximation [56].

A classical test case widely used in the literature is the natural convection over a cylinder immersed in a square cavity. A complete description of the problem is given by Fig. 4a. The system consists of a square enclosure, filled with fluid at rest. Non-slip is assumed in the walls of the cavity and in the interface between the cylinder and the fluid. Initially, the fluid has no solute diluted, i.e., $C(\boldsymbol{x}, 0) = 0$. At $t > 0$, the wall concentration of solute in the circular cylinder and at the enclosure walls are set to C_C and C_E, respectively. Since $C_E > C_C$, mass transfer starts to occur, and the system is treated as a binary mixture. The solute diffuses in the fluid over time, causing mass stratification.

Density gradients can exist in binary mixtures due to gradients in the concentration [57]. Thus, an Oberbeck-Boussinesq approximation can be written for mass transport phenomena, such that a driven body force is proportional to the variation of concentration C, gravity acceleration g and coefficient of mass expansion β. The body force in Eq. (6) takes the form

$$\boldsymbol{F}_{\text{body}} = g\beta\Delta C\,\hat{\boldsymbol{e}}_y, \tag{31}$$

where $\Delta C = C - C_{\text{ref}}$, C_{ref} is a reference concentration and $\hat{\boldsymbol{e}}_y$ is the y-direction component of the standard basis, $(\hat{\boldsymbol{e}}_x, \hat{\boldsymbol{e}}_y, \hat{\boldsymbol{e}}_z)$.

The problem was addressed by multiple authors, usually considering it as natural convection of heat [58–61]. Some works also explored convection in different geometries, including super-elliptical [59] and squared-shaped [62] cylinders, as well as cubical [63] and rectangular cavities [64].

In order to validate results with the work of Moukalled and Acharya [58], the equations are rendered dimensionless, using the reference groups proposed by Gray and Giorgini [56]

$$x_o = L, \tag{32}$$
$$v_o = \sqrt{g\beta L\Delta C}, \tag{33}$$
$$t_o = x_o/v_o, \tag{34}$$
$$\Delta C_o = C_C - C_E, \tag{35}$$
$$P_o = \rho_o v_o^2, \tag{36}$$

where ρ_o is a reference density, considered here as unity. Using these groups, Eqs. (5)–(7) read

$$\frac{\partial \rho^*}{\partial t^*} = -\rho^*\nabla^*\cdot\boldsymbol{v}^*, \tag{37}$$
$$\frac{\partial \boldsymbol{v}^*}{\partial t^*} = -\frac{1}{\rho^*}\nabla^* p^* + \frac{1}{\sqrt{Gr}}\nabla^{*2}\boldsymbol{v}^* + C^*\hat{\mathbf{e}}_y, \tag{38}$$
$$\frac{\partial C^*}{\partial t^*} = \frac{1}{\sqrt{Gr}Sc}\nabla^{*2}C^*, \tag{39}$$

where Gr and Sc denote the Grashof and Schmidt numbers, respectively. The mass transfer Rayleigh number Ra can therefore be defined as

$$Ra = GrSc = \frac{g\beta\Delta C L^3}{\nu\kappa}, \tag{40}$$

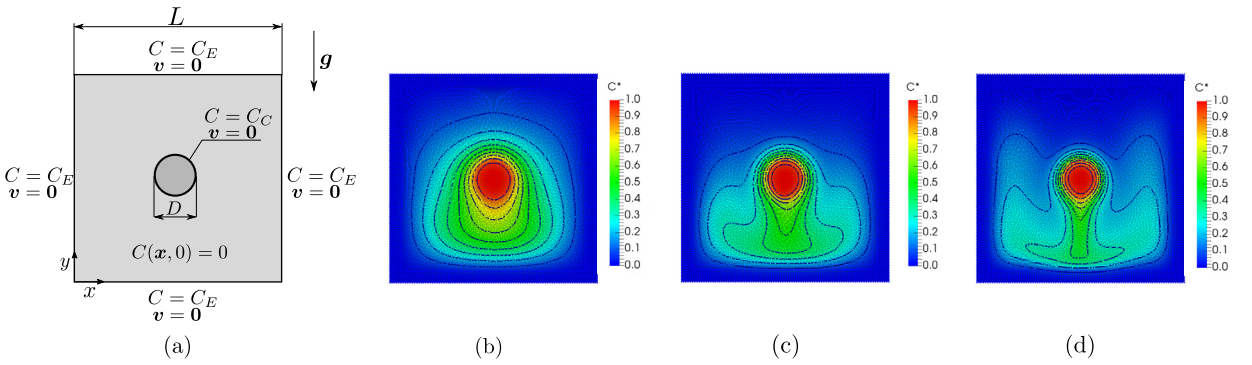

Fig. 4. (a) Schematic of natural convection in a cylinder inside a square enclosure. (b), (c) and (d) show isocontour plots of dimensionless concentration C^* at steady-state, for (b) $Ra = 10^4$, (c) $Ra = 10^5$ and (d) $Ra = 10^6$. Results shown in (b), (c) and (d) were interpolated using a Gaussian kernel, for clarity purposes.

Table 2
Natural convection in a cylinder inside a square enclosure: estimated errors in the concentration (C^*) and velocity (v_y^*) profiles.

Ra	$\epsilon^{\text{SDPD}}(C^*)$	$\epsilon^{\text{SSA}}(C^*)$	$\epsilon^{\text{SDPD}}(v_y^*)$	$\epsilon^{\text{SSA}}(v_y^*)$
10^4	2.587×10^{-3}	2.205×10^{-3}	0.347	0.347
10^5	2.307×10^{-3}	2.447×10^{-3}	1.373	1.409
10^6	3.222×10^{-3}	2.867×10^{-3}	4.378	4.666

thus one can rewrite Eqs. (37)–(39) as

$$\frac{\partial \rho^*}{\partial t^*} = -\rho^* \nabla^* \cdot \boldsymbol{v}^*, \tag{41}$$

$$\frac{\partial \boldsymbol{v}^*}{\partial t^*} = -\nabla^* p^* + \sqrt{\frac{Sc}{Ra}} \nabla^{*2} \boldsymbol{v}^* + C^* \hat{\mathbf{e}}_y, \tag{42}$$

$$\frac{\partial C^*}{\partial t^*} = \frac{1}{\sqrt{RaSc}} \nabla^{*2} C^*. \tag{43}$$

The problem now depends only on Ra and Sc. Following Moukalled and Acharya [58], we take $D = 0.2L$. Simulations were performed for $Ra = 10^4, 10^5$ and 10^6. The Schmidt number was taken to be equal to 0.7.

The range of Rayleigh numbers selected was chosen as a way to test the ability of the present method to predict the onset of the convective plumes and their consequent concentration inversions, which are characteristics of regimes with moderately high Rayleigh numbers ($Ra > 10^5$).

A total of six numerical simulations were performed. For each value of Ra, mass diffusion was resolved using SDPD (cases 1–3) and SSA (cases 4–6). For all the cases, the same number of particles N and same initial conditions were provided. The initial setup consists of $N = 81^2$ equally-spaced particles distributed in a squared domain of length $L = 1$. Boundary conditions are imposed using several layers of stationary particles with fixed concentrations. To guarantee stability, a time step of $\Delta t^* = 10^{-5}$ was used. All the results were averaged in $N_R = 100$ realizations after reaching a sufficiently long simulation time ($t^* \sim 50$).

Profiles of the dimensionless concentration, C^*, and y-velocity component, v_y^*, are shown in Figs. 5a–5b. Results were compared with the numerical simulation of Moukalled and Acharya [58]. Since Moukalled and Acharya [58] uses a different normalization for the velocity, the dimensionless velocity $\boldsymbol{v}^*$ obtained from the solution of Eq. (42) must be re-scaled, by multiplying $\boldsymbol{v}^*$ by $\sqrt{Ra/Sc}$.

In Fig. 5a, for $Ra = 10^4$, the concentration profile decreases monotonically as the distance from the cylinder increases, as observed in Moballa et al. [65]. For $Ra = 10^5$, the concentration profile flattens between the wall and the cylinder surface, due to the formation of boundary layers in these regions, confirming the ability of the present method to correctly predict diffusion in near-wall regions. Similarly, for $Ra = 10^6$, the method was able to capture the stratification [58] of the concentration profile that causes the flow to slow down in the interval $0.65 \lesssim x^* \lesssim 0.85$ (cf. Fig. 5b).

Results for the y-velocity profile are compared in Fig. 5b. A qualitative good agreement was observed for $Ra = 10^4$ and $Ra = 10^5$. For $Ra = 10^6$, significant errors in the near-wall regions were observed, in particular in the neighborhood of the right-wall, indicating excessive viscous damping in these regions, possibly caused by the artificial viscosity term used in the SPH and SDPD formulations. These errors, however, do not seem to affect the mass diffusion with the same intensity, as the concentration profiles in Fig. 5a show good agreement with the reference, even for $Ra = 10^6$.

The differences in magnitude between concentration and velocity errors becomes more evident with the error estimates provided in Table 2. For the concentration profiles, Table 2 show that both SSA and SDPD diffusion-driven errors remain in

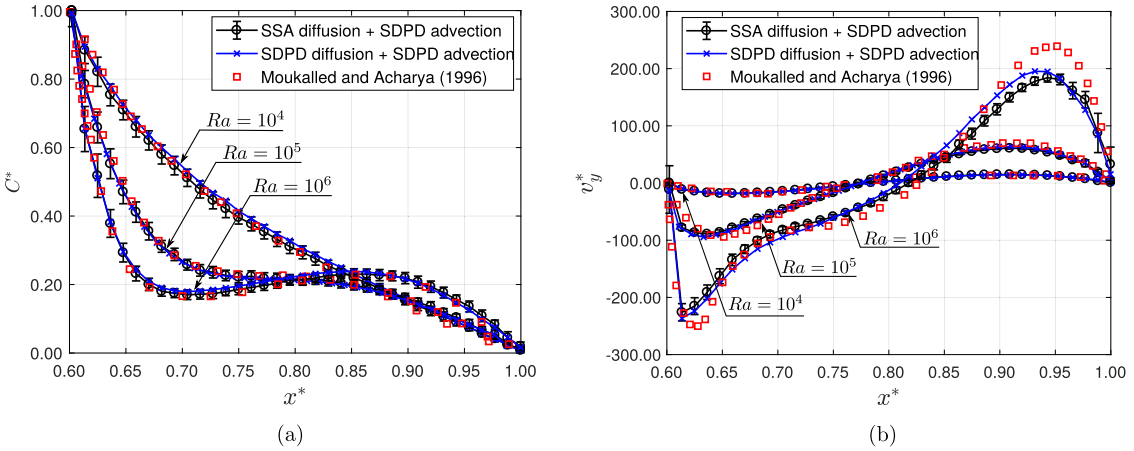

Fig. 5. (a) Comparison of the mean dimensionless concentration (C^*) and (b) dimensionless (re-scaled by $\sqrt{Ra/Sc}$) y-velocity (v_y^*) centerline profiles, for $Ra = 10^4, 10^5$ and 10^6, computed at $t = 50$, over $N_r = 100$ realizations.

Table 3
Dimensional parameters used in the micro-channel numerical experiment.

Parameter	Description	Value
κ_L	α-factor (L) diffusivity	347 [$\mu m^2/s$]
ν	kinematic viscosity	10^{-6} [m^2/s]
$C_L\|_{x=0}$	L concentration at inlet	1.0 [mol/m^3]
$C_R\|_{\text{cell}}$	R concentration at cell wall	1.0 [mol/m^3]
k_{RL}	kinetic association rate	1.0 [$m^3/(mol \cdot s)$]
k_{RLm}	kinetic dissociation rate	1.0 [s^{-1}]
D	diameter of the cell	5.0 [μm]
H	channel height	100.0 [μm]
L_{channel}	channel length	200.0 [μm]
L_{cell}	streamwise cell position	25.0 [μm]
l_{cell}	thickness of cell membrane	1.0 [μm]
v_o	reference velocity	2.5×10^{-4} [m/s]
x_o	reference length	H[m/s]

mol/m^3 is the molar concentration.

the $\mathcal{O}(10^{-3})$, with the error increasing with the increase of Ra. It is important to highlight that, for $Ra = 10^6$, the SSA error was smaller than the SDPD error, showing the potential of the method.

For the velocity errors, shown in Table 2, SDPD seem to perform better than SSA. However, it is important to highlight that advection was modeled using SDPD in both cases. Thus, the error in the velocity is most likely to be caused by the SDPD formulation, and not by SSA mass transport.

4.3. Application: micro-channel reactive flow past a cell

We apply our methodology to perform a challenging simulation of biological significance representing a reactive micro-channel flow past a yeast cell that combines advection, diffusion, and reaction. The typical experiment, depicted schematically in Fig. 6a, consists of a microfluidics chamber with cells immersed in a liquid working medium. The system, initially at rest, starts to experience mixing when at $t > 0$ two different fluids start to flow along the channel from different inlets. A solution containing working fluid and a diluted species (the mating pheromone alpha-factor, denoted by L) is released through one of the inlets, while through the other inlet, working fluid alone is injected into the system (Fig. S3).

As the flow develops, L reacts with the alpha-factor receptor R located at the cell surface, producing a third species, RL (receptor bound to ligand). We assume that the association reaction, $R + L \to RL$ occurs at a rate $k_{RL}[R][L]$. Similarly, the dissociation reaction $RL \to R + L$ also takes place in the system, and occurs at a rate $k_{RLm}[RL]$.

A general deterministic mathematical model that describes the system is given by Eqs. (5)–(7) which can be conveniently written in a non-dimensional form. The reference parameters, evaluated using the dimensional parameters described in Table 3, are given by:

$$x_o = H, \tag{44}$$

$$v_o = x_o/t_o, \tag{45}$$

Table 4
Dimensionless groups used in the numerical experiment.

Group	Description	Value
Da_{I}	first Damköhler number	28.82
Da_{II}	second Damköhler number	28.82
Pe	mass Péclet number	72.06
Re	Reynolds number	2.5×10^{-2}

$$C_o = C_L|_{x=0}, \tag{46}$$

$$P_o = \rho_o v_o^2, \tag{47}$$

where $H, C_L|_{x=0}$ and ρ_o are respectively the channel height, the concentration of alpha-factor at the inlet, and a reference density, considered here as unity. Using these dimensionless groups, Eqs. (5)–(7) are written as

$$\frac{\partial \rho^*}{\partial t^*} = -\rho^* \nabla^* \cdot \boldsymbol{v}^*, \tag{48}$$

$$\frac{\partial \boldsymbol{v}^*}{\partial t^*} = -\frac{1}{\rho^*}\nabla^* p^* + \frac{1}{Re}\nabla^2 \boldsymbol{v}^*, \tag{49}$$

$$\frac{\partial}{\partial t}\begin{bmatrix} C_R^* \\ C_L^* \\ C_{RL}^* \end{bmatrix} = \frac{1}{Pe}\nabla^{*2}\begin{bmatrix} C_R^* \\ C_L^* \\ C_{RL}^* \end{bmatrix} + \begin{bmatrix} R_R^* \\ R_L^* \\ R_{RL}^* \end{bmatrix}, \tag{50}$$

where R_A^*, R_B^* and R_C^* are given by the law of mass action as

$$\begin{bmatrix} R_R^* \\ R_L^* \\ R_{RL}^* \end{bmatrix} = \begin{bmatrix} -1 & 1 \\ -1 & 1 \\ 1 & -1 \end{bmatrix}\begin{bmatrix} C_R^* C_L^* & 0 \\ 0 & C_{RL}^* \end{bmatrix}\begin{bmatrix} Da_{\mathrm{I}}/Pe \\ Da_{\mathrm{II}}/Pe \end{bmatrix}. \tag{51}$$

The system now depends only on four dimensionless groups: $Da_{\mathrm{I}}, Da_{\mathrm{II}}, Pe$ and Re. In the present work, we define these quantities as

$$Da_{\mathrm{I}} = \frac{\tau_{\mathrm{diff}}}{\tau_{\mathrm{reactI}}} = \frac{x_o^2 k_{RL} C_o}{\kappa_L}, \tag{52}$$

$$Da_{\mathrm{II}} = \frac{\tau_{\mathrm{diff}}}{\tau_{\mathrm{reactII}}} = \frac{x_o^2 k_{RLm}}{\kappa_L}, \tag{53}$$

$$Pe = \frac{x_o v_o}{\kappa_L}, \tag{54}$$

$$Re = \frac{x_o v_o}{\nu}. \tag{55}$$

The first and second Damköhler numbers, denoted by $Da_{\mathrm{I}}, Da_{\mathrm{II}}$, are defined as the ratio between an arbitrary mixing time scale τ_{mix} and the chemical time scale of a n-th order reaction τ_{react}. It is important to highlight that the mixing scale is problem-dependent; for combustion-dominated flows, the mixing scale is related to the turbulent time scale [66,67], whereas in diffusion-dominant problems, the mixing scale is related to the molecular diffusion time scale [68–71].

The mass Péclet number, denoted by Pe, describes the ratio of advection and molecular diffusion transport [70,72]. Similarly, the Reynolds number Re describes the ratio of inertial to viscous transport in the flow[72].

The problem was solved using three different approaches: the present method, i.e., hybrid sSSA-SDPD, SDPD, and the finite element method (FEM). All of the cases were computed using the parameters described in Tables 3–4. Both hybrid sSSA-SDPD and SDPD simulations were performed using $N = 1250$ particles. The number of molecules per particle was taken as $N_m = 1600$. Note that because of the low level of parallelism of the SSA algorithm, simulations of the hybrid method must run in serial, which restricts the maximum number of particles involved in the simulation, as well as the number of realizations. As an example, we show only one SSA realization. The finite element problem was modeled using the software Comsol Multiphysics (v5.2a), using second-order shape functions in a mesh of approximately 17000 elements. Equations (49)–(50) were solved assuming incompressibility.

A qualitative comparison between the concentration of alpha-factor, C_L, is depicted in Fig. 6b. At time $t^* = 2$, results show qualitative agreement. A mixing layer is formed in the first half of the channel, with the hybrid method showing a delay in the frontal concentration when compared with FEM solution, indicating differences in the velocity field. As the flow contours around the cell, the mixing layer is interrupted, causing a separation of the concentration field into two fronts.

Fig. 6c provides a quantitative comparison between the algorithms. The y^*-centerline profiles of C_{RL}^* shown in Fig. 6c demonstrate that despite its low resolution, the hybrid method still captured the physics of the problem. Note that the

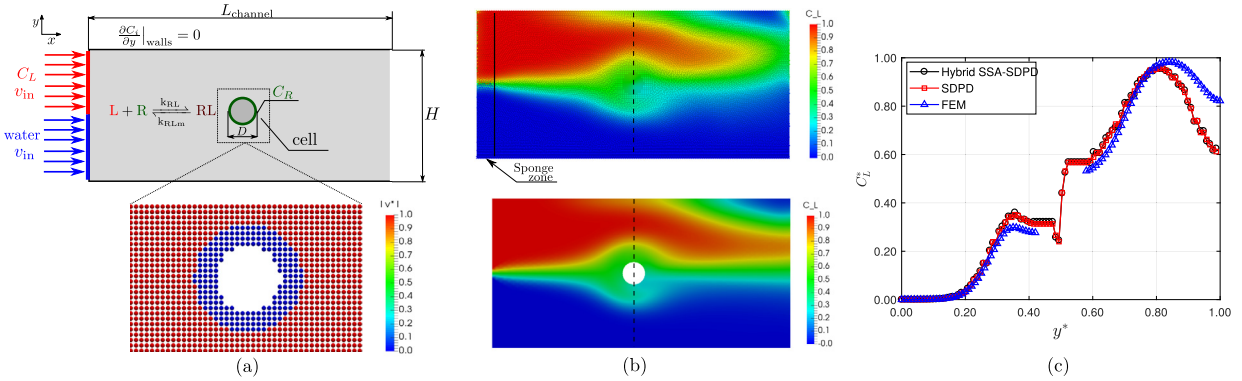

Fig. 6. (a) Upper: schematic of our model of a yeast cell in a microfluidics channel flow containing a pheromone gradient. The working fluid is initially at rest, and at time $t > 0$, two inlets start to inject fluid into the chamber; the upper inlet consists of a diluted mixture of working fluid and alpha-factor L, and the lower inlet injects working fluid in the system. (a) Lower: magnified region around the cell, illustrating the particles and their initial velocities. (b) Contour plots of the dimensionless concentration of alpha-factor, C_L^*, at $t^* = 2$, obtained using the proposed hybrid method (upper) and FEM (lower). (c) Comparison of the dimensionless concentration profiles of alpha-factor, C_L^*, between hybrid sSSA-SDPD, SDPD and finite element method (FEM), measured across the y^* centerline, at time $t^* = 2$. Results shown in (b) were interpolated using a Gaussian kernel, for clarity purposes.

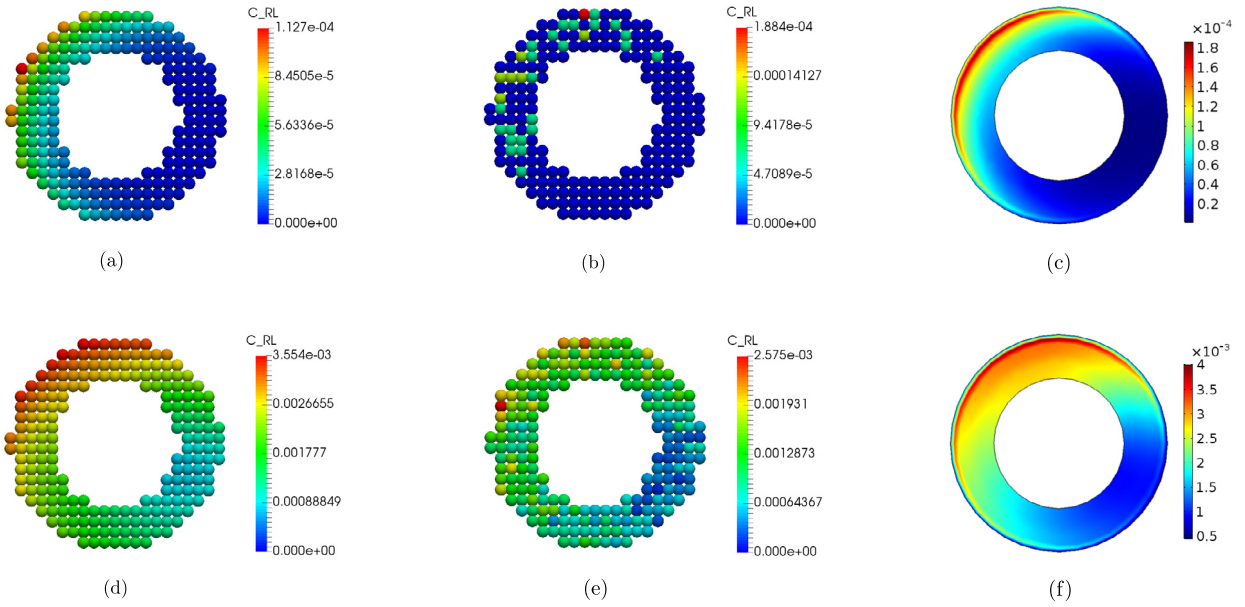

Fig. 7. Top: dimensionless concentration of species RL at the cell wall, C_{RL}^*, at $t^* = 1$ (equivalent to physical time $t = 0.4[s]$), obtained by: (a) SDPD, (b) hybrid sSSA-SDPD method and (c) finite element method. Bottom: dimensionless concentration of species RL at the cell wall, C_{RL}^*, at $t^* = 2$ (equivalent to physical time $t = 0.8[s]$), obtained by: (d) SDPD, (e) sSSA-SDPD method and (f) finite element method. Note that the deterministic SDPD simulations in (a) and (d) match closely the finite element results in (c) and (f). However, the sSSA-SDPD simulations in (b) and (e) are able to capture the discrete stochastic dynamics of this subcellular biological process.

curves are in phase with each other. Still in Fig. 6c, it is noticeable that results are in far better agreement with FEM at regions away from the boundaries. A possible cause of this discrepancy originates from the way non-slip boundary conditions are imposed. For simplicity, in this example, the cell was modeled using stationary particles, which may introduce errors due to the boundary curvature [73]. In particular, the usage of more sophisticated boundary treatments have shown to be effective in improving stability and accuracy of simulations [73,74].

Finally, a comparison of the formation of species RL in the cell wall region for all three methods is shown in Fig. 7. Results show that SSA results can significantly differ from SDPD and FEM, depending on the species concentrations involved and number of realizations performed. The explanation for the differences between the hybrid sSSA-SDPD method and FEM results depend on how significant the stochastic effects are, and how well the PDEs used in FEM and the SDEs of SDPD can describe the reaction–diffusion process.

The discrepancies observed in Fig. 7 illustrate a case where stochastic effects are relevant enough that deterministic methods can no longer predict the physics of the problem accurately. Furthermore, this typical biological problem shows that

it is not always obvious when stochastic effects are important, as the continuum hypothesis might hold true for momentum transport, but not for reactive mass transfer. The proposed hybrid method, however, allows for the correct representation of the physics of this class of problems. In particular, the method bridges the gap between stochastic and deterministic advection–diffusion–reaction systems in biological applications. Thus, the hybrid sSSA-SDPD method enables the simulation of systems spanning a large range of Knudsen numbers, without any *ad hoc* assumption about the Knudsen number or the relevance of stochastic transport.

5. Conclusion

We have developed a method to simulate both discrete stochastic and continuum deterministic chemical reaction–diffusion systems within an unstructured moving fluid domain whose dynamics are simulated via the smoothed dissipative particle dynamics method. This method has many applications where chemically or biochemically reactive systems are coupled to a moving fluid domain. For example, it will be especially useful for modeling biological cells in which discrete stochastic chemical kinetics are required to accurately describe cellular processes.

It is important to emphasize that because of the Lagrangian nature of SDPD, the coupling with advective transport occurs naturally, with particle positions being updated via the equations of motion. This approach has been proven to work in different scales, ranging from relativistic spaces [75] to quantum systems [76]. Thus, our method preserves the natural advantages of a meshfree method while incorporating the flexibility of resolving small scales only when necessary, making it a complete framework for the simulation of biological multiscale systems.

We use operator splitting to couple the SDPD dynamics of fluid position and velocity, the continuum deterministic reaction–diffusion equations, and SSA discrete stochastic reaction–diffusion system over each timestep. This allows us to solve a complex interdependent system efficiently and simply, with known error bounds [77,78].

We have implemented our method within the LAMMPS[52] simulation framework. LAMMPS is a software package for simulation of classical molecular dynamics problems. The advantage of the LAMMPS infrastructure is that is extensible, and has been modified to include simulation capabilities of SPH, and DPD (including tDPD in a recent release). We have implemented the SDPD, deterministic reaction–diffusion, and the spatial SSA methods as a user module in LAMMPS, which should allow it to be integrated seamlessly into many different configurations of LAMMPS. We have released the source for our enhancements under the GPL v2.0 license, which is the same license as the LAMMPS software package. For ease of replication of our results, we have packaged the solver and our examples as a Docker container https://hub.docker.com/r/briandrawert/hybrid_ssa_sdpd/. Directions on how to use this container and the full source code are found on Github: https://github.com/briandrawert/hybrid_SSA_SDPD.

Our simulation methodology has many advantages, but there are still technical limitations. There are issues in specifying boundary conditions when using the SSA simulation method, as it is not as straightforward to specify them in the discrete context compared to the continuous context. In addition, the current implementation of the SSA method requires that the simulations be run in serial, rather than utilizing multi-core parallelism. This is due to the fully connected nature of the SSA method. Our plans for future work include adapting the SSA method to the multi-core parallel context to increase performance.

We believe that this method will lead to advances in the understanding of complex systems. Specifically, we envision its application in the modeling of single cell and multicellular systems possessing changing shapes in dynamic environments subjected to various perturbations. Applications such as this require coupling between physical and chemical systems, a simulation our method is designed to address. For example, sSSA-SDPD is able to simulate both the complex fluid dynamics and the stochastic biochemical reactions of cells in a microfluidics chamber. Finally, we can use the algorithm to model the physical forces and blood flow in tissues coupled to inter- and intra-cellular processes.

Acknowledgements

The authors acknowledge research funding from the Brazilian National Research Council (CNPq) through Grant No. 209793/2014-7, and by National Institutes of Health (NIH) NIGMS Award No. R01-GM113241 and NIH Award No. R01-EB014877. We acknowledge support from the NSF Center for Scientific Computing from the CNSI, MRL: an NSF MRSEC (DMR-1121053) and NSF CNS-0960316 for computational resources. The content of the information does not necessarily reflect the position or the policy of the funding agencies, and no official endorsement should be inferred.

Appendix A. Supplementary material

Supplementary material related to this article can be found online at https://doi.org/10.1016/j.jcp.2018.10.043.

References

[1] P. Español, P. Warren, Perspective: dissipative particle dynamics, J. Chem. Phys. 146 (2017) 150901.
[2] Z. Li, A. Yazdani, A. Tartakovsky, G.E. Karniadakis, Transport dissipative particle dynamics model for mesoscopic advection–diffusion–reaction problems, J. Chem. Phys. 143 (2015) 014101.
[3] M.B. Elowitz, A.J. Levine, E.D. Siggia, P.S. Swain, Stochastic gene expression in a single cell, Science 297 (2002) 1183–1186.

[4] B. Drawert, S. Hellander, M. Trogdon, T.-M. Yi, L. Petzold, A framework for discrete stochastic simulation on 3d moving boundary domains, J. Chem. Phys. 145 (2016) 184113.
[5] S.P. Banavar, C. Gomez, M. Trogdon, L.R. Petzold, T.-M. Yi, O. Campàs, Mechanical feedback coordinates cell wall expansion and assembly in yeast mating morphogenesis, PLoS Comput. Biol. 14 (2018) e1005940.
[6] T.-R. Teschner, L. Könözsy, K.W. Jenkins, Progress in particle-based multiscale and hybrid methods for flow applications, Microfluid. Nanofluid. 20 (2016) 68.
[7] G. Karniadakis, A. Beskok, N. Aluru, Microflows and Nanoflows: Fundamentals and Simulation, Interdisciplinary Applied Mathematics, Springer, New York, 2005.
[8] S. Litvinov, M. Ellero, X. Hu, N.A. Adams, Smoothed dissipative particle dynamics model for polymer molecules in suspension, Phys. Rev. E 77 (2008) 066703.
[9] S. Litvinov, M. Ellero, X. Hu, N.A. Adams, Self-diffusion coefficient in smoothed dissipative particle dynamics, J. Chem. Phys. 130 (2009) 021101.
[10] G. Faure, J.-B. Maillet, J. Roussel, G. Stoltz, Size consistency in smoothed dissipative particle dynamics, Phys. Rev. E 94 (2016) 043305.
[11] P.J. Hoogerbrugge, J.M.V.A. Koelman, Simulating microscopic hydrodynamic phenomena with dissipative particle dynamics, EPL Europhys. Lett. 19 (1992) 155.
[12] P. Español, P. Warren, Statistical mechanics of dissipative particle dynamics, EPL Europhys. Lett. 30 (1995) 191.
[13] J.D. Moore, B.C. Barnes, S. Izvekov, M. Lísal, M.S. Sellers, D.E. Taylor, J.K. Brennan, A coarse-grain force field for RDX: density dependent and energy conserving, J. Chem. Phys. 144 (2016) 104501.
[14] A. Chaudhri, J.R. Lukes, Multicomponent energy conserving dissipative particle dynamics: a general framework for mesoscopic heat transfer applications, J. Heat Transf. 131 (2009) 033108.
[15] E. Abu-Nada, Dissipative particle dynamics simulation of natural convection using variable thermal properties, Int. Commun. Heat Mass Transf. 69 (2015) 84–93.
[16] E.O. Johansson, T. Yamada, B. Sundén, J. Yuan, Modeling mesoscopic solidification using dissipative particle dynamics, Int. J. Therm. Sci. 101 (2016) 207–216.
[17] M. Liu, P. Meakin, H. Huang, Dissipative particle dynamics simulation of pore-scale multiphase fluid flow, Water Resour. Res. 43 (2007) W04411.
[18] Y. Xia, J. Goral, H. Huang, I. Miskovic, P. Meakin, M. Deo, Many-body dissipative particle dynamics modeling of fluid flow in fine-grained nanoporous shales, Phys. Fluids 29 (2017) 056601.
[19] G.C. Ganzenmuller, S. Hiermaier, M.O. Steinhauser, Shock-wave induced damage in lipid bilayers: a dissipative particle dynamics simulation study, Soft Matter 7 (2011) 4307–4317.
[20] J.B. Maillet, E. Bourasseau, N. Desbiens, G. Vallverdu, G. Stoltz, Mesoscopic simulations of shock-to-detonation transition in reactive liquid high explosive, EPL Europhys. Lett. 96 (2011) 68007.
[21] A. Vázquez-Quesada, M. Ellero, P. Español, Consistent scaling of thermal fluctuations in smoothed dissipative particle dynamics, J. Chem. Phys. 130 (2009) 034901.
[22] J.A. Backer, C.P. Lowe, H.C.J. Hoefsloot, P.D. Iedema, Combined length scales in dissipative particle dynamics, J. Chem. Phys. 123 (2005) 114905.
[23] R. Qiao, P. He, Mapping of dissipative particle dynamics in fluctuating hydrodynamics simulations, J. Chem. Phys. 128 (2008) 126101.
[24] P. Español, M. Revenga, Smoothed dissipative particle dynamics, Phys. Rev. E 67 (2003) 026705.
[25] D. Bernstein, Simulating mesoscopic reaction–diffusion systems using the Gillespie algorithm, Phys. Rev. E 71 (2005) 041103.
[26] J. Elf, M. Ehrenberg, Spontaneous separation of bi-stable biochemical systems into spatial domains of opposite phases, in: Systems Biology, IEE Proceedings, vol. 1, IET, 2004, pp. 230–236.
[27] A.B. Stundzia, C.J. Lumsden, Stochastic simulation of coupled reaction–diffusion processes, J. Comput. Phys. 127 (1996) 196–207.
[28] C.W. Gardiner, et al., Handbook of Stochastic Methods, vol. 3, Springer, Berlin, 1985.
[29] N.D. Petsev, L.G. Leal, M.S. Shell, Hybrid molecular-continuum simulations using smoothed dissipative particle dynamics, J. Chem. Phys. 142 (2015) 044101.
[30] F. Irgens, Continuum Mechanics, Springer, Berlin Heidelberg, 2008.
[31] J.J. Monaghan, Smoothed particle hydrodynamics, Rep. Prog. Phys. 68 (2005) 1703.
[32] M.B. Liu, G.R. Liu, Smoothed particle hydrodynamics (SPH): an overview and recent developments, Arch. Comput. Methods Eng. 17 (2010) 25–76.
[33] X. Xu, X.-L. Deng, An improved weakly compressible SPH method for simulating free surface flows of viscous and viscoelastic fluids, Comput. Phys. Commun. 201 (2016) 43–62.
[34] L.B. Lucy, A numerical approach to the testing of the fission hypothesis, Astron. J. 82 (1977) 1013–1024.
[35] M. Ellero, P. Español, E.G. Flekkøy, Thermodynamically consistent fluid particle model for viscoelastic flows, Phys. Rev. E 68 (2003) 041504.
[36] D. Molteni, A. Colagrossi, A simple procedure to improve the pressure evaluation in hydrodynamic context using the SPH, Comput. Phys. Commun. 180 (2009) 861–872.
[37] S. Shao, E.Y. Lo, Incompressible SPH method for simulating Newtonian and non-Newtonian flows with a free surface, Adv. Water Resour. 26 (2003) 787–800.
[38] J.J. Monaghan, Smoothed particle hydrodynamics, Annu. Rev. Astron. Astrophys. 30 (1992) 543–574.
[39] M. Grmela, H.C. Öttinger, Dynamics and thermodynamics of complex fluids. I. Development of a general formalism, Phys. Rev. E 56 (1997) 6620.
[40] H.C. Öttinger, M. Grmela, Dynamics and thermodynamics of complex fluids. II. Illustrations of a general formalism, Phys. Rev. E 56 (1997) 6633.
[41] S. Lind, R. Xu, P. Stansby, B. Rogers, Incompressible smoothed particle hydrodynamics for free-surface flows: a generalised diffusion-based algorithm for stability and validations for impulsive flows and propagating waves, J. Comput. Phys. 231 (2012) 1499–1523.
[42] M. Ellero, M. Serrano, P. Español, Incompressible smoothed particle hydrodynamics, J. Comput. Phys. 226 (2007) 1731–1752.
[43] J. Monaghan, J. Kajtar, SPH particle boundary forces for arbitrary boundaries, Comput. Phys. Commun. 180 (2009) 1811–1820.
[44] S. Adami, X. Hu, N. Adams, A transport-velocity formulation for smoothed particle hydrodynamics, J. Comput. Phys. 241 (2013) 292–307.
[45] G. Oger, M. Doring, B. Alessandrini, P. Ferrant, An improved SPH method: towards higher order convergence, J. Comput. Phys. 225 (2007) 1472–1492.
[46] J. Monaghan, SPH without a tensile instability, J. Comput. Phys. 159 (2000) 290–311.
[47] N. Barkai, S. Leibler, Biological rhythms: circadian clocks limited by noise, Nature 403 (2000) 267–268.
[48] J. Paulsson, O.G. Berg, M. Ehrenberg, Stochastic focusing: fluctuation-enhanced sensitivity of intracellular regulation, Proc. Natl. Acad. Sci. 97 (2000) 7148–7153.
[49] M. Thattai, A. Van Oudenaarden, Intrinsic noise in gene regulatory networks, Proc. Natl. Acad. Sci. 98 (2001) 8614–8619.
[50] D.T. Gillespie, Exact stochastic simulation of coupled chemical reactions, J. Phys. Chem. 81 (1977) 2340–2361.
[51] A.M. Tartakovsky, P. Meakin, T.D. Scheibe, R.M.E. West, Simulations of reactive transport and precipitation with smoothed particle hydrodynamics, J. Comput. Phys. 222 (2007) 654–672.
[52] S. Plimpton, Fast parallel algorithms for short-range molecular dynamics, J. Comput. Phys. 117 (1995) 1–19.
[53] B. Drawert, B. Jacob, Z. Li, T.-M. Yi, L. Petzold, Validation data for a hybrid smoothed dissipative particle dynamics (SDPD) spatial stochastic simulation algorithm (sSSA) method, Data Brief. (2018), in press.

[54] B. Drawert, A. Hellander, B. Bales, D. Banerjee, G. Bellesia, B.J. Daigle Jr., G. Douglas, M. Gu, A. Gupta, S. Hellander, C. Horuk, D. Nath, A. Takkar, S. Wu, P. Lötstedt, C. Krintz, L.R. Petzold, Stochastic simulation service: bridging the gap between the computational expert and the biologist, PLoS Comput. Biol. 12 (2016) 1–15.
[55] S.K. Lele, Compact finite difference schemes with spectral-like resolution, J. Comput. Phys. 103 (1992) 16–42.
[56] D.D. Gray, A. Giorgini, The validity of the boussinesq approximation for liquids and gases, Int. J. Heat Mass Transf. 19 (1976) 545–551.
[57] H.D.H.D. Baehr, Heat and Mass Transfer, 3rd ed., Springer, Heidelberg, New York, 2011.
[58] F. Moukalled, S. Acharya, Natural convection in the annulus between concentric horizontal circular and square cylinders, J. Thermophys. Heat Transf. 10 (1996) 524–531.
[59] C. Shu, Y.D. Zhu, Efficient computation of natural convection in a concentric annulus between an outer square cylinder and an inner circular cylinder, Int. J. Numer. Methods Fluids 38 (2002) 429–445.
[60] Y. Peng, Y.T. Chew, C. Shu, Numerical simulation of natural convection in a concentric annulus between a square outer cylinder and a circular inner cylinder using the Taylor-series-expansion and least-squares-based lattice Boltzmann method, Phys. Rev. E 67 (2003) 026701.
[61] D. Angeli, P. Levoni, G.S. Barozzi, Numerical predictions for stable buoyant regimes within a square cavity containing a heated horizontal cylinder, Int. J. Heat Mass Transf. 51 (2008) 553–565.
[62] A.K. De, A. Dalal, A numerical study of natural convection around a square, horizontal, heated cylinder placed in an enclosure, Int. J. Heat Mass Transf. 49 (2006) 4608–4623.
[63] C. Butler, D. Newport, M. Geron, Natural convection experiments on a heated horizontal cylinder in a differentially heated square cavity, Exp. Therm. Fluid Sci. 44 (2013) 199–208.
[64] G. Cesini, M. Paroncini, G. Cortella, M. Manzan, Natural convection from a horizontal cylinder in a rectangular cavity, Int. J. Heat Mass Transf. 42 (1999) 1801–1811.
[65] B. Moballa, M.-J. Chern, E. Odhiambo, Incompressible smoothed particle hydrodynamics modeling of thermal convection, Interact. Multiscale Mech. 6 (2013).
[66] M. Mungal, C. Frieler, The effects of Damköhler number in a turbulent shear layer, Combust. Flame 71 (1988) 23–34.
[67] N.E.L. Haugen, J. Kruger, D. Mitra, T. Lovas, The effect of turbulence on mass transfer rates of small inertial particles with surface reactions, J. Fluid Mech. 836 (2018) 932–951.
[68] L. Schmidt, The Engineering of Chemical Reactions, Topics in Chemical Engineering, Oxford University Press, 1998.
[69] J. Plawsky, Transport Phenomena Fundamentals, Chemical Industries, Taylor & Francis, 2001.
[70] I. Tosun, Modelling in Transport Phenomena, Elsevier Science, 2002.
[71] R. Kee, M. Coltrin, P. Glarborg, Chemically Reacting Flow: Theory and Practice, Wiley, 2005.
[72] T. Bennett, Transport by Advection and Diffusion, Wiley Global Education, 2012.
[73] J.P. Morris, P.J. Fox, Y. Zhu, Modeling low Reynolds number incompressible flows using SPH, J. Comput. Phys. 136 (1997) 214–226.
[74] S. Adami, X. Hu, N. Adams, A generalized wall boundary condition for smoothed particle hydrodynamics, J. Comput. Phys. 231 (2012) 7057–7075.
[75] S. Rosswog, Boosting the accuracy of SPH techniques: Newtonian and special-relativistic tests, Mon. Not. R. Astron. Soc. 448 (2015) 3628–3664.
[76] P. Mocz, S. Succi, Numerical solution of the nonlinear Schrödinger equation using smoothed-particle hydrodynamics, Phys. Rev. E 91 (2015) 053304.
[77] A. Hellander, M.J. Lawson, B. Drawert, L. Petzold, Local error estimates for adaptive simulation of the reaction–diffusion master equation via operator splitting, J. Comput. Phys. 266 (2014) 89–100.
[78] T. Jahnke, C. Lubich, Error bounds for exponential operator splittings, BIT Numer. Math. 40 (2000) 735–744.